Experimental determination of Ramsey numbers with quantum annealing

Zhengbing Bian,[1] Fabian Chudak,[1] William G. Macready,[1] Lane Clark,[2] and Frank Gaitan[3]

[1] *D-Wave Systems, Inc., 100-4401 Still Creek Drive, Burnaby, British Columbia V5C 6G9, Canada*
[2] *Department of Mathematics, Southern Illinois University, Carbondale, IL 62901-4401*
[3] *Laboratory for Physical Sciences, 8050 Greenmead Dr, College Park, MD 20740*

(Dated: January 11, 2012)

Ramsey theory is a highly active research area in mathematics that studies the emergence of order in large disordered structures. It has found applications in mathematics, theoretical computer science, information theory, and classical error correcting codes. Ramsey numbers mark the threshold at which order first appears and are notoriously difficult to calculate due to their explosive rate of growth. Recently, a quantum algorithm has been proposed that calculates the two-color Ramsey numbers $R(m, n)$. Here we present results of an experimental implementation of this algorithm based on quantum annealing and show that it correctly determines the Ramsey numbers $R(3, 3)$ and $R(m, 2)$ for $4 \leq m \leq 8$. The $R(8, 2)$ computation used 84 qubits of which 28 were computational qubits. This computation is the largest experimental implementation of a scientifically meaningful quantum algorithm that has been done to date.

PACS numbers: 03.67.Ac,02.10.Ox,89.75.Hc

arXiv:1201.1842v2 [quant-ph] 10 Jan 2012

In recent years first steps have been taken towards the goal of experimentally realizing the computational advantages promised by well-known quantum algorithms. As with any nascent effort, these initial steps have been limited. To date the largest experimental implementations of scientifically meaningful quantum algorithms have used just a handful of qubits. For circuit-based algorithms,[1] *seven* spin-qubits were used to factor 15; while for adiabatic quantum algorithms,[2] *four* spin-qubits were used to factor 143. In *both* cases specialized versions of the quantum algorithms were needed to allow factoring with such small numbers of qubits. Although factoring was the focus of both experiments, other scientifically significant applications exist.

In Ref. 3 a quantum algorithm was proposed for determining the notorious two-color Ramsey numbers. Experimental implementation of this algorithm offers significant challenges as it requires, even for the smallest Ramsey numbers, a considerable number of *non-local*, *high-order* qubit couplings. Because of these challenges, Ramsey numbers are an excellent testbed for quantum hardware.

Ramsey numbers are part of an active research area in mathematics known as Ramsey theory[4] whose central theme is the emergence of order in large disordered structures. Problems in Ramsey theory often have an intuitive character that is easily grasped. For example, imagine that we decide to throw a party. We would like the party-size N to be large enough that either there will be a group of m people who all know each other (and can get the party started), or a group of n people who are mutual strangers (and so must mingle, again getting the party started). Using Ramsey theory[4,5], it can be shown that a threshold value $R(m, n)$ exists so that as long as the party-size N is not less than $R(m, n)$, *every* party of N people will contain either m mutual acquaintances or n mutual strangers. The threshold value $R(m, n)$ is an example of a two-color Ramsey number. Other types of Ramsey numbers exist, though we will focus on two-color Ramsey numbers here.

Ramsey numbers grow extremely quickly and are notoriously difficult to calculate. For (two-color) Ramsey numbers $R(m, n)$ with $m, n \geq 3$, only nine are presently known[5]. To dramatize the difficulty of calculating $R(m, n)$, Spencer recounts a famous vignette due to Paul Erdös[6] in which aliens have invaded earth and threaten to destroy it in one year unless humans can correctly determine $R(5, 5)$. Erdös noted that this could probably be done if all the best minds and most powerful computers were focused on the task. In this case, the appropriate response to the alien demand would be to get busy. However, Erdös pointed out that if the aliens had instead demanded $R(6, 6)$ (viz. incrementing m and n by 1), earthlings should immediately launch a first-strike on the aliens as there is little hope of meeting their demand.

In the Ramsey number quantum algorithm[3] (RQA) the calculation of $R(m, n)$ is formulated as an optimization problem which is solved using quantum adiabatic evolution.[7] Here we present results of an *experimental* implementation of the RQA based on quantum annealing and show that it correctly determines the Ramsey numbers $R(3, 3)$ and $R(m, 2)$ for $4 \leq m \leq 8$. The experimental computation of $R(8, 2)$ used a total of 84 qubits of which 28 were computational qubits, and applied an effective interaction coupling 28 qubits. To the best of our knowledge, this is the largest experimental implementation of a scientifically meaningful quantum algorithm.

We begin this report with a brief description of the RQA. We then discuss the experimental details of implementing the RQA on a chip of 106 superconducting flux qubits using quantum annealing, and follow with a presentation of our experimental results. Finally, we close with a summary of what has been found.

1. Quantum algorithm: To start, notice that our N-person party problem can be represented by an N-vertex graph. We associate a vertex with each person,

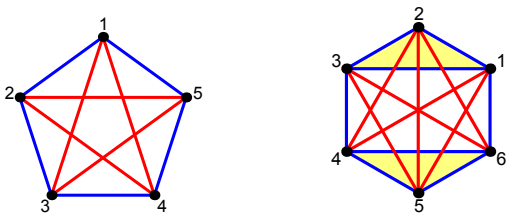

(a) $N = 5$ (b) $N = 6$

FIG. 1: **Two-colored graphs and the party problem.** These 5- and 6-vertex graphs represent instances of parties with 5 and 6 people. Pairs of acquaintances are joined by blue edges, and pairs of strangers by red edges. (a) This graph with $N = 5$ has no red or blue 3-cliques (i.e. triangles) corresponding to a party where no group of 3 people are mutual friends or strangers. (b) This graph with $N = 6$ contains two blue triangles (with yellow interiors) corresponding to two separate groups of 3 mutual friends. Ramsey theory guarantees the impossibility of coloring the edges of such 6-vertex graphs without creating at least one red or blue triangle.

and an edge is drawn between a pair of vertices only when the corresponding people know each other. For m mutual acquaintances, an edge will connect any pair of the m corresponding vertices, while for n mutual strangers, there will be no edge between any two of the n corresponding vertices. The m vertices are said to form an m-clique and the n vertices an n-independent set. Our party problem is now a statement about graphs: every graph with $N \geq R(m,n)$ vertices contains an m-clique or an n-independent set. Note that any N-vertex graph can be converted into a fully-connected N-vertex graph with two-colored edges by replacing each edge with a blue edge and each missing edge with a red edge. This transforms m-cliques into blue m-cliques and n-independent sets into red n-cliques (see Fig. 1).

We briefly describe the construction of the RQA (see Ref. 3 and the Supplementary Information (SI) for a detailed presentation). As computation of $R(m,n)$ is intimately connected with the presence/absence of edges, we associate a bit-variable $a_{v,v'}$ with each pair of vertices (v,v') in an N-vertex graph G. Bit-variable $a_{v,v'} = 1$ (0) when v and v' are (are not) joined by an edge in G. There are thus $L_N = \binom{N}{2} \equiv N(N-1)/2$ bit-variables which we collect into the bit-vector (bit-string) $\boldsymbol{a} = (a_{2,1} \cdots, a_{N,1}, a_{3,2}, \cdots, a_{N,2}, \cdots, a_{N,N-1})$ of length L_N. Notice that an N-vertex graph G determines a unique bit-string $\boldsymbol{a}$, and vice versa[3].

Ref. 3 (and the SI) showed how to count the number of m-cliques $C_m^N(\boldsymbol{a})$ and n-independent sets $I_n^N(\boldsymbol{a})$ in an N-vertex graph G using its associated bit-string $\boldsymbol{a}$. Thus for any (N-vertex) graph G, $h_{m,n}^N(\boldsymbol{a}) = C_m^N(\boldsymbol{a}) + I_n^N(\boldsymbol{a})$ is the total number of m-cliques and n-independent sets contained in G. It follows that $h_{m,n}^N(\boldsymbol{a})$ must be greater than or equal to zero, and $h_{m,n}^N(\boldsymbol{a}) = 0$ if (and only if) $G_{\boldsymbol{a}}$ has no m-cliques or n-independent sets.

The next step in construction of the RQA is to use $h_{m,n}^N(\boldsymbol{a})$ as the cost function for the following combinatorial optimization problem (COP): For given integers (N,m,n) and cost function $h_{m,n}^N(\boldsymbol{a})$ defined as above, find an N-vertex graph $G_{\boldsymbol{a}_\star}$ that yields the global minimum of $h_{m,n}^N(\boldsymbol{a})$. Notice that if $N < R(m,n)$, the global minimum is $h_{m,n}^N(\boldsymbol{a}_\star) = 0$ since Ramsey theory guarantees that a graph exists that has no m-clique or n-independent set. Furthermore, if $N \geq R(m,n)$, Ramsey theory guarantees that $h(\boldsymbol{a}_\star) > 0$. If we begin with $N < R(m,n)$ and increment N by 1 until we first find $h_{m,n}^N(\boldsymbol{a}_\star) > 0$, then the corresponding N will be exactly $R(m,n)$. We will return to this observation shortly.

Adiabatic quantum optimization (AQO)[7] exploits the adiabatic evolution of a quantum system to solve a COP, and quantum annealing (QA) provides a physical means of implementing AQO. The resultant QA algorithm is comparable to simulated annealing[8], but relies on quantum fluctuations instead of thermal fluctuations. The QA algorithm uses the COP cost function to define a problem Hamiltonian H_P whose ground-state eigenspace contains all COP solutions. The QA algorithm evolves the state of an L_N qubit register from the ground-state of an initial Hamiltonian H_i to a ground-state of H_P with probability approaching 1 in the adiabatic limit. The time-dependent Hamiltonian $H(t)$ driving the QA algorithm is $H(t) = A(t/t_f)H_i + B(t/t_f)H_P$, where t_f is the algorithm run-time, and adiabatic dynamics corresponds to $t_f \to \infty$. Here $A(t/t_f)$ ($B(t/t_f)$) is a positive monotonically decreasing (increasing) function with $A(1) = 0$ ($B(0) = 0$).

To convert the Ramsey COP into a AQO/QA computation, each of the bit-variables $a_{v,v'}$ is promoted to a qubit, thus associating a qubit with each vertex pair (v,v'). The bit-strings $\boldsymbol{a}$ now label the computational basis (CB) states $|\boldsymbol{a}\rangle$, and the Ramsey problem Hamiltonian H_P is defined to be diagonal in the CB with eigenvalue $h_{m,n}^N(\boldsymbol{a})$. By construction, the ground-state energy of H_P vanishes if (and only if) there is a graph with no m-cliques or n-independent sets. The initial Hamiltonian H_i is the standard one for AQO[7] and appears in the SI. Its unique ground-state is the uniform superposition of all CB states which is easy to prepare experimentally.

The quantum algorithm for computing $R(m,n)$ begins by choosing N to be a strict lower bound of the Ramsey number: $N < R(m,n)$. The QA algorithm is run on L_N qubits and the energy E is measured at the end of algorithm execution. In the adiabatic limit the result will be $E = 0$ since $N < R(m,n)$. The value of N is incremented $N \to N+1$, the QA algorithm is re-run on L_{N+1} qubits, and the final energy is measured. This process is repeated until $E > 0$ first occurs, at which point the current value of N will be equal to $R(m,n)$. In any real application of the QA algorithm the evolution will only be approximately adiabatic. Thus the probability the measured energy will be the ground-state energy will be $1-\epsilon$. To circumvent this, the QA algorithm must be run $k \sim \mathcal{O}(\ln[1-\delta]/\ln\epsilon)$ times so that with probability $\delta > 1-\epsilon$, at least one of the measurement outcomes will

be the ground-state energy. By making k large enough, δ can be brought arbitrarily close to 1.

For experimental implementation of Ramsey AQO the bit-vector $\boldsymbol{a}$ must be transformed to the spin-vector $\boldsymbol{s} = 2\boldsymbol{a} - 1$ so that $a_{v,v'} = 1\,(0)$ maps to $s_{v,v'} = 1\,(-1)$. In a slight abuse of notation we write $C_m^N(\boldsymbol{s}) \equiv C_m^N\big((1+\boldsymbol{s})/2\big)$, $I_n^N(\boldsymbol{s}) \equiv I_n^N\big((1+\boldsymbol{s})/2\big)$, and $h_{m,n}^N(\boldsymbol{s}) = C_m^N(\boldsymbol{s}) + I_n^N(\boldsymbol{s})$.

2. Experimental constraints: Our hardware implementation of QA uses RF SQUID flux qubits. Each qubit is a superconducting loop interrupted by Josephson junctions, and the states $|0\rangle$ and $|1\rangle$ correspond to the two directions of circulating current about the loop.[9] The chip hardware uses Josephson-junction-based devices to produce pairwise qubit-coupling.[10] The low energy dynamics of the chip is well-described by a quantum Ising model in a transverse field with Hamiltonian:

$$H = A\left(\frac{t}{t_f}\right)\sum_i \sigma_i^x + B\left(\frac{t}{t_f}\right)\left\{\sum_i h_i\sigma_i^z + \sum_{(i,j)\in E} J_{ij}\sigma_i^z\sigma_j^z\right\}.$$

As the qubit couplers are physical devices with definite locations on the chip, there are constraints on the qubit coupling/connectivity. Fig. 2(a) shows the layout of qubits and couplers on the chip. The local biases $\{h_i\}$ and coupling strengths $\{J_{ij}\}$ may be programmed to values in the ranges $[-2, 2]$ and $[-1, 1]$ respectively, and the experimentally measured functional forms of the interpolation functions $A(t/t_f)$ and $B(t/t_f)$ appear in the SI. For further details of the chip hardware, see Ref. 11.

The cost function $h_{m,n}^N(\boldsymbol{s})$ is still not ready for experimental implementation for two reasons: (a) there are k-spin interactions with $k > 2$; and (b) the spin couplings do not correspond to the qubit couplings in Fig. 2(a). These obstacles are removed as follows.

(*a*) *Reduction to pairwise coupling:* The SI shows that $C_m^N(\boldsymbol{s})$ involves interactions coupling $\binom{m}{2}$ spins, while $I_n^N(\boldsymbol{s})$ couples $\binom{n}{2}$ spins. These interactions must be reduced to pairwise coupling if $h_{m,n}^N(\boldsymbol{s})$ is to be realized experimentally. We illustrate how such a reduction can be achieved by reducing the 3-bit coupling term $a_1a_2a_3$ to pairwise coupling using an ancillary bit-variable b and penalty function

$$P(a_1, a_2; b) = a_1a_2 - 2(a_1 + a_2)b + 3b. \qquad (1)$$

Notice that $P(a_1, a_2; b) = 0$ (> 0) when the input values for a_1, a_2, and b satisfy $b = a_1a_2$ $(b \neq a_1a_2)$. Now consider the quadratic cost function $h(b) = ba_3 + \mu P(a_1a_2; b)$ for given values of μ and a_i. For μ sufficiently large, $h(b)$ is minimized when b satisfies the equality constraint $b = a_1a_2$ which causes the penalty function to vanish. The optimum cost is then $h(b = a_1a_2) = a_1a_2a_3$ which reproduces the 3-bit coupling term using a *quadratic* cost function. This example is generalized in Sec. 3 to produce the quadratic cost function used to calculate $R(m, 2)$.

(*b*) *Matching spin to qubit connectivity:* A cost function with only pairwise spin coupling may still not be experimentally realizable as the spin couplings needed may not match the qubit couplings available on chip. The primal graph (PG) of a quadratic cost function is the graph whose vertices are the spin variables, and whose edges indicate pairwise-coupled spins. An arbitrary PG can be embedded into a sufficiently large qubit graph having the structure of Fig. 2(a). An embedding maps a PG vertex to one or more vertices in the qubit graph, where the image vertices form a connected subgraph of the qubit graph. We link this connected set of qubits together with strong ferromagnetic couplings so that in the lowest energy state these qubits have identical Bloch vectors. For example, to couple qubits 104 and 75 in Fig. 2(a) (which are not directly coupled) with coupling strength $\mathcal{J}$, we ferromagnetically couple qubits 104, 112, and 107 using strongly negative $J_{104,112}$ and $J_{107,112}$ values. The desired coupling is then carried along the edge

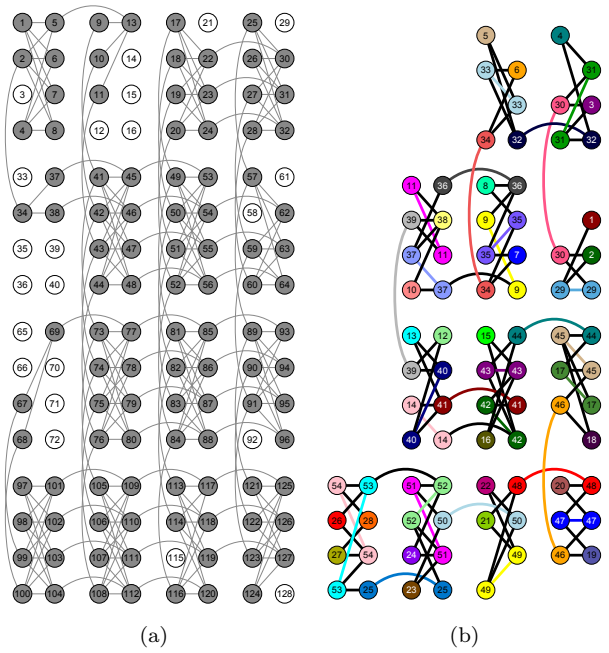

(a) (b)

FIG. 2: **(a) Layout of qubits and couplers.** The chip architecture is a 4×4 array of unit cells, with each unit cell containing 8 qubits. Within a unit cell, each of the 4 qubits in the left-hand partition (LHP) connects to all 4 qubits in the right-hand partition (RHP), and vice versa. A qubit in the LHP (RHP) also connects to the corresponding qubit in the LHP (RHP) of the units cells above and below (to the left and right of) it. Qubits are labeled from 1 to 128, and edges between qubits represent couplers with programmable coupling strengths. Grey qubits indicate usable qubits, while white qubits indicate qubits that could not be calibrated to operating tolerances and were not used. All experiments were done on a chip with 106 usable qubits. **(b) R(8, 2) embedding for qubit connectivity.** Embedding used to compute $R(8, 2)$ that produced the needed qubit couplings. In low energy states like-colored qubits have the same Bloch vector and constitute a single effective qubit. This allows an indirect coupling of qubits that are not directly coupled in hardware.

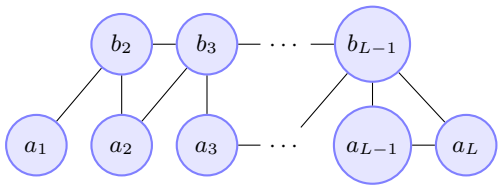

FIG. 3: **Primal graph for $C_m^m(\boldsymbol{a},\boldsymbol{b})$.** The penalty function $P(\boldsymbol{a};\boldsymbol{b})$ imposes the constraints $b_{L-1} = a_{L-1}a_L$ and $b_j = a_j b_{j+1}$. The primal graph displays the pairwise couplings appearing in $C_m^m(\boldsymbol{a};\boldsymbol{b}) = a_1 b_2 + \mu\, P(\boldsymbol{a};\boldsymbol{b})$.

connecting qubits 107 and 75 with $J_{75,107} = \mathcal{J}$.

3. Ramsey energy functions: We considered a number of Ramsey problems which could be solved using the 106 qubits available in Fig. 2(a). Specifically, $R(m,2)$ with $4 \le m \le 8$ and $R(3,3)$.

(a) $R(m,2)$: Since an N-vertex graph $G_{\boldsymbol{a}}$ with $N < m$ cannot contain an m-clique, it follows that $C_m^N(\boldsymbol{a}) = 0$ for all $G_{\boldsymbol{a}}$. Thus, for $N < m$, $h_{m,2}^N(\boldsymbol{a}) = I_2^N(\boldsymbol{a}) = \overline{a}_1 + \cdots + \overline{a}_{L_N}$, where $\overline{a}_i = 1 - a_i$. This produces a problem Hamiltonian H_P with L_N *uncoupled* qubits which is easily mapped onto the chip. Now consider $N = m$. Defining $L = L_m = \binom{m}{2}$, we have $C_m^m(\boldsymbol{a}) = a_1 a_2 \cdots a_{L-1} a_L$, and $h_{m,2}^m(\boldsymbol{a}) = C_m^m(\boldsymbol{a}) + I_2^m(\boldsymbol{a})$. The L-bit interaction in $C_m^m(\boldsymbol{a})$ is reduced to pairwise coupling by introducing: (i) ancillary bit variables $b_2, \cdots, b_{L-1}$, and (ii) imposing the constraints $b_{L-1} = a_{L-1}a_L$ and $b_j = a_j b_{j+1}$ $(j = 2, \cdots, L-2)$ through the penalty function $P(\boldsymbol{a};\boldsymbol{b}) = P(a_{L-1}, a_L; b_{L-1}) + \sum_{j=2}^{L-2} P(a_j, b_{j+1}; b_j)$ (see Eq. (1)). The $R(m,2)$ cost function for $N = m$ is then $h_{m,2}^m(\boldsymbol{a},\boldsymbol{b}) = \{a_1 b_2 + \mu\, P(\boldsymbol{a};\boldsymbol{b})\} + I_2^m(\boldsymbol{a})$, where $\mu = 2$ is the penalty weight value used in all $R(m,2)$ experiments. Making the substitutions $2\boldsymbol{a} = \boldsymbol{s}_a + 1$ and $2\boldsymbol{b} = \boldsymbol{s}_b + 1$ expresses the cost function in terms of Ising spin variables.

The PG for pairwise interactions present in $h_{m,2}^m(\boldsymbol{a},\boldsymbol{b})$ appears in Fig. 3. We have embedded this PG into the hardware up to $N = m = 8$. In Fig. 2(b) we display the embedding that was used to determine $R(8,2)$, and which used 28 computational qubits, 26 ancilla qubits to reduce interactions to pairwise, and 30 qubits to match the PG connectivity in Fig. 3 to the qubit connectivity in Fig. 2(b) for a total of 84 qubits.

(b) $R(3,3)$: We also determined $R(3,3)$ by examining $N = 4, 5, 6$. The cost functions for these cases are

$$
\begin{aligned}
h_{3,3}^4(\boldsymbol{a}) &= f_{1,2,4} + f_{1,3,5} + f_{2,3,6} + f_{4,5,6};\\
h_{3,3}^5(\boldsymbol{a}) &= f_{1,2,5} + f_{1,3,6} + f_{1,4,7} + f_{2,3,8} + f_{2,4,9} +\\
&\quad f_{3,4,10} + f_{5,6,8} + f_{5,7,9} + f_{6,7,10} + f_{8,9,10};\\
h_{3,3}^6(\boldsymbol{a}) &= f_{1,2,6} + f_{1,3,7} + f_{1,4,8} + f_{1,5,9} + f_{2,3,10} + f_{2,4,11}\\
&\quad + f_{2,5,12} + f_{3,4,13} + f_{3,5,14} + f_{4,5,15} + f_{6,7,10}\\
&\quad + f_{6,8,11} + f_{6,9,12} + f_{7,8,13} + f_{7,9,14} + f_{8,9,15}\\
&\quad + f_{10,11,13} + f_{10,12,14} + f_{11,12,15} + f_{13,14,15};
\end{aligned}
$$

where $f_{i,j,k} = a_i a_j a_k + \overline{a}_i \overline{a}_j \overline{a}_k$. Notice that $f_{i,j,k}$ can be re-written as $f_{i,j,k} = -2 + \overline{a}_i + \overline{a}_j + \overline{a}_k + a_i a_j + a_i a_k + a_j a_k$, which only contains *pairwise* couplings, making ancillary $\boldsymbol{b}$-spins unnecessary. The largest of these problems is $N = 6$ whose PG has 15 vertices and 60 edges. We can reduce its size slightly by exploiting the identity $h_{m,n}^N(\boldsymbol{a}) = h_{n,m}^N(\overline{\boldsymbol{a}})$. For $m = n$ this yields a two-fold symmetry: if $\boldsymbol{a}_\star$ is a global minimum of $h_{m,m}^N$, so is $\overline{\boldsymbol{a}}_\star$. Thus, we can fix one variable (say $a_1 = 0$) and optimize over the remaining variables $\boldsymbol{a}'$. Optimal solutions then have the form $(0, \boldsymbol{a}'_\star)$ and $(1, \overline{\boldsymbol{a}}'_\star)$. With this simplification, the PG of $h_{3,3}^6(0, \boldsymbol{a}')$ has 14 vertices and 52 edges. The SI shows its embedding into the chip hardware.

4. Results: To solve a given Ramsey COP specified by the parameters $\boldsymbol{h}$ and $\boldsymbol{J}$, the chip must first be programmed to fix these values in hardware. For the largest problem we solved ($R(8,2)$ using 84 qubits) this took roughly 270 ms. After programming we iterate many cycles of annealing and readout. Each annealing cycle has duration $t_f = 1$ ms, and readout of the qubits takes 1.5 ms per sample. Programming only occurs once so the total runtime required to obtain S Ramsey output samples is $270 + (1 + 1.5)S$ ms. As the hardware is an analog device, there is limited precision to which $\boldsymbol{h}$ and $\boldsymbol{J}$ can be specified. For a COP whose ground state is sensitive to parameter settings this could pose serious difficulties. However, the Ramsey COP requires specification of only a few distinct integral values, and ground states are quite stable to parameter perturbations.

Although most discussions of QA assume zero-temperature, all experiments here were performed at 20 mK, or roughly 0.4 GHz. For comparison, peak values of the interpolation functions $A(t/t_f)$ and $B(t/t_f)$ are of order 10 GHz (see the SI). Refs. 12,13 show that finite temperature need not destroy the efficacy of QA. In our experiments we select the lowest energy configuration observed over many annealing cycles to compensate for the stochastic influence of non-zero temperature.

Figs. 4 and 5 present our results for $R(8,2)$ and $R(3,3)$. The SI contains our results for $R(m,2)$ with $m = 4, \cdots, 7$ which could not be included here due to space limitations. Both Figures display histograms that plot the relative-frequency of energy values obtained by programming the chip and running 10^5 annealing and readout cycles, yielding 10^5 $\boldsymbol{s}$-spin configurations. In the main figures, histograms of the energies of the Ising problem sent to the hardware are plotted. These Ising cost functions include the Ramsey cost function $h_{m,n}^N(\boldsymbol{s})$, and the ferromagnetic penalties enforcing the equality constraints amongst qubits that represent the same PG spin variable. The ferromagnetic penalty weight λ was adjusted so that at least 85% of output $\boldsymbol{s}$-configurations satisfied the equality constraints. These feasible spin configurations were translated back to the original $\boldsymbol{a}$ variables and the cost/energy function $h_{m,n}^N(\boldsymbol{a})$ evaluated. The resulting energy values were binned and plotted in the inset histograms.

Fig. 4 presents our results for $R(8,2)$ which was the

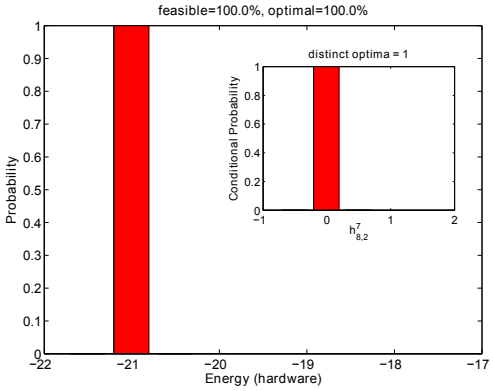

(a) $N = 7$

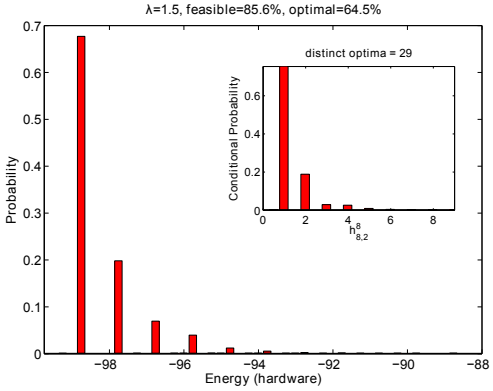

(b) $N = 8$

FIG. 4: **Energy histograms for $R(8, 2)$** on graphs below $(N = 7)$ and at $(N = 8)$ the Ramsey transition.

largest of the $R(m, 2)$ problems considered. Of the $\boldsymbol{s}$-configurations returned by the hardware for $N = 8$, approximately 65% are global minima of $h^8_{8,2}$. Examining the inset histograms for $N = 7$ (8) we see that: (i) $h_{min} = 0$ (1); (ii) the probability for $h = 0$ (1) is approximately 1.0 (0.65); and (iii) the number of optimal $\boldsymbol{a}$-configurations/graphs is 1 (29). The energies h_{min} found for $N = 7$ and 8 agree with the final ground-state (GS) energies found in Ref. 3, indicating that QA finds the final GS with high-probability. As h_{min} jumps from $0 \to 1$ as N goes from $7 \to 8$, the Ramsey protocol correctly[5] identifies $R(8, 2) = 8$. Finally, Ref. 3 showed that the number of optimal graphs for $N = 7$ (8) is 1 (29) which agrees with what was found by QA. For $N = 7$, the unique optimal $\boldsymbol{a}$-configuration corresponds to the graph in which every pair of vertices is connected by an edge and so has no 2-independent sets or 8-clique and so has $h^7_{8,2} = 0$. For $N = 8$, the 29 optimal $\boldsymbol{a}$-configurations correspond to graphs $G_{\boldsymbol{a}}$ with $h^8_{8,2}(\boldsymbol{a}) = 1$ which are the twenty-eight 8-vertex graphs containing a single 2-independent set, and the single 8-vertex graph containing an 8-clique.

We also examined $R(3, 3)$ with $N = 4, 5, 6$. Fig. 5 shows our results for $N = 5$ and 6, while $N = 4$ appears

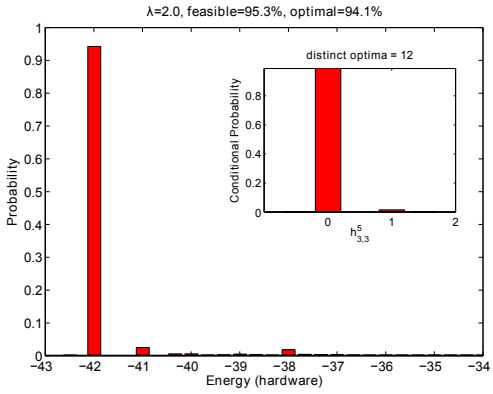

(a) $N = 5$

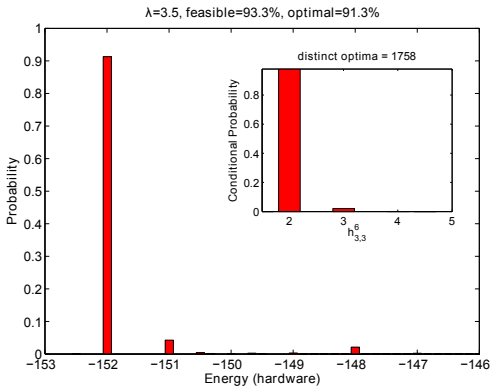

(b) $N = 6$

FIG. 5: **Energy histograms for $R(3, 3)$** on graphs below $(N = 5)$ and at $(N = 6)$ the Ramsey transition.

in the SI. Together, they show that the minimum energies for $N = 4, 5, 6$ are $0, 0, 2$, respectively, and these occur with probabilities of approximately 0.93, 0.94, and 0.91. The energies h_{min} agree with the final GS energies found in Ref. 3 indicating that QA again finds the final GS with high-probability. As h_{min} jumps from $0 \to 2$ as N goes from $5 \to 6$, the Ramsey protocol correctly[5] identifies $R(3, 3) = 6$. Finally, Ref. 3 showed that the number of optimal graphs for $N = 4, 5, 6$ is $18, 12, 1760$, respectively, in excellent agreement with the QA results of $18, 12, 1758$.

5. Summary: We presented results of an experimental implementation of a quantum algorithm that computes two-color Ramsey numbers $R(m, n)$[3]. We showed that the algorithm correctly determined $R(m, 2) = m$ for $4 \leq m \leq 8$, and $R(3, 3) = 6$. A summary of our results, along with corresponding theoretical predictions, appear in Table I. The $R(8, 2)$ computation used 84 qubits of which 28 were computational qubits, and to the best of our knowledge is the largest experimental implementation of a scientifically meaningful quantum algorithm.

TABLE I: **Results**[1] **for Ramsey numbers** $R(m,2)=m$ **for** $4 \leq m \leq 8$ **and** $R(3,3)=6$**.**

$\mathbf{R(2,4)}$			$\mathbf{R(2,5)}$			$\mathbf{R(2,6)}$			$\mathbf{R(2,7)}$			$\mathbf{R(2,8)}$			$\mathbf{R(3,3)}$		
N	E_{gs}	D	N	E_{gs}	D	N	E_{gs}	D	N	E_{gs}	D	N	E_{gs}	D	N	E_{gs}	D
3	0(0)	1(1)	4	0(0)	1(1)	5	0(0)	1(1)	6	0(0)	1(1)	7	0(0)	1(1)	5	0(0)	12(12)
4	1(1)	7(7)	5	1(1)	11(11)	6	1(1)	16(16)	7	1(1)	22(22)	8	1(1)	29(29)	6	2(2)	1758(1760)

[1] N is the number of graph vertices; E_{gs} and D are the ground-state energy and degeneracy, respectively, for the problem Hamiltonian H_P; and for each Ramsey number, the experimental results are followed by the theoretical predictions from Ref. 3 in parenthesis.

[1] Vandersypen, L.M.K. et al.. Experimental realization of Shor's quantum factoring algorithm using nuclear magnetic resonance. *Nature* **414**, 883–887 (2001).

[2] Xu, N. et al.. Quantum factorization of 143 on a dipolar-coupling NMR system. Preprint at http://arxiv.org/abs/1111.3726v1 (2011).

[3] Gaitan, F. & Clark, L.. Ramsey numbers and adiabatic quantum computing. *Phys. Rev. Lett.* **108**, 010501 (2012).

[4] Graham, R. L., Rothschild, B. L., & Spencer, J. H.. *Ramsey Theory* (John Wiley & Sons, New York, 1990).

[5] Bollobás, B.. *Modern Graph Theory* (Springer, New York, 1998).

[6] Spencer, J.. *Ten Lectures on the Probabalistic Method*, 2nd ed. (SIAM, Philidelphia, 1994).

[7] Farhi, E., Goldstone, J., Gutmann, S., & Sipser, M.. Quantum computation by adiabatic evolution. Preprint at http://arxiv.org/abs/quant-ph/0001106 (2000).

[8] Kirkpatrick, S., Gelatt, C. D., & Vecchi, M. P.. Optimization by simulated annealing. *Science* **220** 671-680 (1983).

[9] Harris, R. et al.. Experimental demonstration of a robust and scalable flux qubit. *Phys. Rev. B* **81**, 134510 (2010).

[10] Harris, R. et al.. A compound Josephson junction coupler for flux qubits with minimal crosstalk. *Phys. Rev. B* **80**, 052506 (2009).

[11] Johnson, M. W. et al.. Quantum annealing with manufactured spins. *Nature* **473**, 194–198 (2011).

[12] Amin, M. H. S., Love, P. J., & Truncik, C. J. S.. Thermally assisted adiabatic quantum computation. *Phys. Rev. Lett.* **100**, 060503 (2008).

[13] Amin, M. H. S., Truncik, C. J. S., & Averin, D. V.. Role of single qubit decoherence time in adiabatic quantum computation. *Phys. Rev. A* **80**, 022303 (2009).

Acknowledgements We thank the D-Wave hardware team for providing this experimental platform, and F. G. thanks T. Howell III for continued support.

Author Contributions Z.B., F.C., and W.G.M. carried out the experiments; L.C. and F.G. contributed to the theoretical analysis; and W.G.M. and F.G. wrote the manuscript.

Supplementary Information for "Experimental determination of Ramsey numbers with quantum annealing"

Zhengbing Bian,[1] Fabian Chudak,[1] William G. Macready,[1] Lane Clark,[2] and Frank Gaitan[3]

[1]*D-Wave Systems, Inc., 100-4401 Still Creek Drive, Burnaby, British Columbia V5C 6G9, Canada*
[2]*Department of Mathematics, Southern Illinois University, Carbondale, IL 62901-4401*
[3]*Laboratory for Physical Sciences, 8050 Greenmead Dr, College Park, MD 20740*

(Dated: January 11, 2012)

In this Supplement we briefly review the construction of the Ramsey number quantum algorithm, and present those Ramsey number experimental results that could not be included in the manuscript due to space limitations. We also present two examples of embeddings of the Ramsey problem Hamiltonian H_P into the chip hardware. These embeddings explicitly show how qubit couplings are laid out on the chip so as to reproduce the couplings appearing in the problem Hamiltonian H_P.

PACS numbers: 03.67.Ac,02.10.Ox,89.75.Hc

arXiv:1201.1842v2 [quant-ph] 10 Jan 2012

The structure of this Supplementary Information (SI) is as follows. We begin in Section I with a description of how the Ramsey number quantum algorithm is constructed. Section II then presents those Ramsey number experimental results that could not be included in the manuscript due to space limitations. Section II A presents the results for $R(3,3)$ with $N=4$, while Section II B presents the results for the Ramsey numbers $R(m,2)$ with $4 \le m \le 7$. For easy reference, Section II A also includes the data for $R(3,3)$ with $N=5$ and 6 which appears in Section 4 of the manuscript. Finally, Section III displays the embedding of the Ramsey energy functions into the chip for $R(3,3)$ with $N=6$ (Section III A) and $R(8,2)$ with $N=8$ (Section III B). These embeddings represent the most complex embeddings we encountered in our experimental determination of, respectively, diagonal ($R(m,m)$) and non-diagonal ($R(m,n)$, $m \neq n$) Ramsey numbers.

I. RAMSEY NUMBER QUANTUM ALGORITHM

We briefly describe the Ramsey number quantum adiabatic algorithm (see Ref. 1 for details). We begin by establishing a 1-1 correspondence between the set of N-vertex graphs and binary strings of length $L = N(N-1)/2$. To each N-vertex graph G there corresponds a unique adjacency matrix $A(G)$ which is an $N \times N$ symmetric matrix with vanishing diagonal matrix elements, and with off-diagonal element $a_{i,j} = 1\,(0)$ when distinct vertices i and j are (are not) joined by an edge. It follows that $A(G)$ is determined by its lower triangular part. By concatenating column-wise the matrix elements $a_{i,j}$ appearing below the principal diagonal, we can construct a unique binary string $g(G)$ of length L for each graph G:

$$g(G) \equiv a_{2,1} \cdots a_{N,1}\; a_{3,2} \cdots a_{N,2}\; \cdots\; a_{N,N-1}. \tag{1}$$

Given the string $g(G)$, the following procedure determines the number of m-cliques in G. Choose m vertices, $S_\alpha = \{v_1, \ldots, v_m\}$, from the N vertices of G and form the product $\mathcal{C}_\alpha = \prod_{(v_j, v_k \in S_\alpha)}^{(j \neq k)} a_{v_j, v_k}$. Note that $\mathcal{C}_\alpha = 1$ when S_α forms an m-clique; otherwise $\mathcal{C}_\alpha = 0$. Now repeat this procedure for all $\rho = C(N,m)$ ways of choosing m vertices from N vertices, and form the sum $\mathcal{C}(G) = \sum_{\alpha=1}^{\rho} \mathcal{C}_\alpha$. By construction, $\mathcal{C}(G)$ equals the number of m-cliques contained in G. A similar procedure determines the number of n-independent sets in G. Briefly, choose n vertices $T_\alpha = \{v_1, \ldots, v_n\}$ from the N vertices in G, and form the product $\mathcal{I}_\alpha = \prod_{(v_j, v_k \in T_\alpha)}^{(j \neq k)} \overline{a}_{v_j, v_k}$, where $\overline{a}_{v_j, v_k} = 1 - a_{v_j, v_k}$. Note that if $\mathcal{I}_\alpha = 1$, then T_α forms an n-independent set; otherwise $\mathcal{I}_\alpha = 0$. Repeat this for all $\nu = C(N,n)$ ways of choosing n vertices from N vertices, then form the sum $\mathcal{I}(G) = \sum_{\alpha=1}^{\nu} \mathcal{I}_\alpha$. By construction, $\mathcal{I}(G)$ gives the number of n-independent sets contained in G. Finally, define

$$h(G) = \mathcal{C}(G) + \mathcal{I}(G). \tag{2}$$

It follows from the above discussion that $h(G)$ is the total number of m-cliques and n-independent sets in G. Thus $h(G) \ge 0$ for all graphs G; and $h(G) = 0$ if and only if G does not contain an m-clique or n-independent set.

We use $h(G)$ as the cost function for the following combinatorial optimization problem. For given integers N, m and n, and with $h(G)$ defined as above, find an N-vertex graph G_* that yields the global minimum of $h(G)$. Notice that if $N < R(m,n)$, the (global) minimum will be $h(G_*) = 0$ since Ramsey theory guarantees that a graph exists which has no m-clique or n-independent set. On the other hand, if $N \ge R(m,n)$, Ramsey theory guarantees $h(G_*) > 0$. If we begin with $N < R(m,n)$ and increment N by 1 until we first find $h(G_*) > 0$, then the corresponding N will be

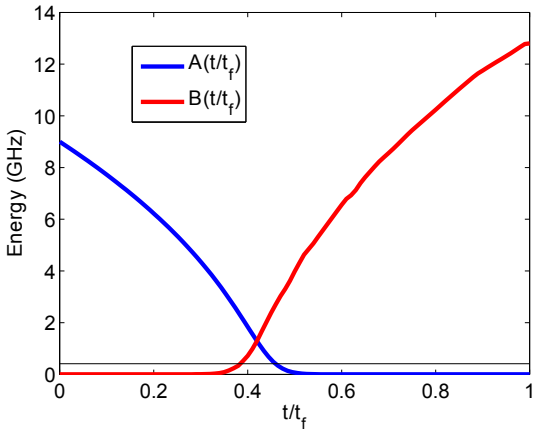

FIG. 1: **Interpolation functions $A(t/t_f)$ and $B(t/t_f)$.** The functional forms of the experimentally measured interpolation functions $A(t/t_f)$ and $B(t/t_f)$ are shown. The QA run-time t_f can be adjusted for times ranging from 20–20 000 μs. For comparison, the temperature at which the experiment is performed is shown as the line at roughly 0.4 GHz.

exactly $R(m,n)$. We now show how this combinatorial optimization problem can be solved using adiabatic quantum evolution, which then becomes the basis for a quantum algorithm to compute $R(m,n)$.

The adiabatic quantum evolution (AQE) algorithm[2] exploits the adiabatic dynamics of a quantum system to solve combinatorial optimization problems. The AQE algorithm uses the optimization problem cost function to define a problem Hamiltonian H_P whose ground-state eigenspace encodes all problem solutions. The algorithm evolves the state of an L-qubit register from the ground-state of an initial Hamiltonian H_i to the ground-state of H_P with probability approaching 1 in the adiabatic limit. An appropriate measurement at the end of the adiabatic evolution yields a solution of the optimization problem almost certainly. The time-dependent Hamiltonian $H(t)$ for local AQE is

$$H(t) = A(t/t_f)H_i + B(t/t_f)H_P, \tag{3}$$

where t_f is the algorithm run-time; adiabatic dynamics corresponds to $t_f \to \infty$; and $A(t/t_f)$ ($B(t/t_f)$) is a positive monotonically decreasing (increasing) function with $A(1) = 0$ ($B(0) = 0$). The experimentally measured functional forms of the interpolation functions $A(t/t_f)$ and $B(t/t_f)$ are shown in Fig. 1.

To map the optimization problem associated with computing $R(m,n)$ onto an adiabatic quantum computation, we begin with the 1-1 correspondence between N-vertex graphs G and length $L = N(N-1)/2$ binary strings $g(G)$. From Eq. (1) we see that position along the string is indexed by the graph edges (i,j). We thus identify a qubit with each vertex pair (i,j), and will thus need L qubits. Defining the computational basis states (CBS) to be the eigenstates of $\sigma_z^0 \otimes \cdots \otimes \sigma_z^{L-1}$, we identify the 2^L graph strings $g(G)$ with the 2^L CBS: $g(G) \to |g(G)\rangle$. The problem Hamiltonian H_P is defined to be diagonal in the computational basis with eigenvalue $h(G)$ associated with eigenstate $|g(G)\rangle$:

$$H_P|g(G)\rangle = h(G)|g(G)\rangle. \tag{4}$$

Note that the ground-state energy of H_P will be zero iff there is a graph with no m-cliques or n-independent sets. An operator expression for H_P appears in Ref. 1. The initial Hamiltonian H_i is chosen to be

$$H_i = \sum_{i=0}^{L-1} \sigma_x^i, \tag{5}$$

where I^i and σ_x^i are, respectively, the identity and x-Pauli operator for qubit i. The ground-state of H_i is the easily constructed uniform superposition of CBS[2].

The quantum algorithm for computing $R(m,n)$ begins by setting N equal to a strict lower bound for $R(m,n)$ which can be found using the probabilistic method[3] or a table of two-color Ramsey numbers[4]. The AQE algorithm is run on $L_N = N(N-1)/2$ qubits, and the energy E is measured at the end of algorithm execution. In the adiabatic limit the result will be $E = 0$ since $N < R(m,n)$. The value of N is incremented $N \to N+1$, the AQE algorithm is re-run on L_{N+1} qubits, and the energy is measured at the end of algorithm execution. This process is repeated until $E > 0$ first occurs, at which point the current value of N will be equal to the $R(m,n)$. Note that any real application of

TABLE I: Results[1] for Ramsey numbers $R(m,2)=m$ for $4 \le m \le 8$ and $R(3,3)=6$.

R(2,4)			**R(2,5)**			**R(2,6)**			**R(2,7)**			**R(2,8)**			**R(3,3)**		
N	E_{gs}	D	N	E_{gs}	D	N	E_{gs}	D	N	E_{gs}	D	N	E_{gs}	D	N	E_{gs}	D
3	0(0)	1(1)	4	0(0)	1(1)	5	0(0)	1(1)	6	0(0)	1(1)	7	0(0)	1(1)	5	0(0)	12(12)
4	1(1)	7(7)	5	1(1)	11(11)	6	1(1)	16(16)	7	1(1)	22(22)	8	1(1)	29(29)	6	2(2)	1758(1760)

[1] N is the number of graph vertices; E_{gs} and D are the ground-state energy and degeneracy, respectively, for the problem Hamiltonian H_P; and for each Ramsey number, the experimental results are followed by the theoretical predictions from Ref. 1 in parenthesis.

AQE will only be approximately adiabatic. Thus the probability that the measured energy E will be the ground-state energy will be $1-\epsilon$. In this case, the algorithm must be run $k \sim \mathcal{O}(\ln[1-\delta]/\ln\epsilon)$ times so that, with probability $\delta > 1-\epsilon$, at least one of the measurement outcomes will be the true ground-state energy. We can make δ arbitrarily close to 1 by choosing k sufficiently large.

II. REMAINING RAMSEY NUMBER RESULTS

Ref. 1 made three predictions that allow theory and experiment to be compared. The first is that the Ramsey number $R(m,n)$ is the value of N at which the global minimum h_{min} of the cost function $h^N_{m,n}(\boldsymbol{a})$ first becomes non-zero. The other two are, respectively, the value of the final ground-state energy $E_{gs} = h_{min} \equiv \min_{\boldsymbol{a}} h^N_{m,n}(\boldsymbol{a})$ and its degeneracy D. For reference, Table I from the manuscript is included below which summarizes all our experimental results and the corresponding theoretical predictions. Examination of the Table shows that there is excellent agreement between the two.

In Secs. II A and II B we present our results for $R(3,3)$ and $R(m,2)$. For each Ramsey number experiment, histograms of the final energies are presented. These energies are determined as follows. At the end of each quantum annealing run, the qubits are measured in the computational basis, and the outcome is the final spin variable-assignment $\boldsymbol{s}$. As explained in Sec. 4 of the manuscript, for those spin configurations satisfying the equality constraints, the spin configuration $\boldsymbol{s}$ is translated back to the original binary $\boldsymbol{a}$ variables. The energy $E(\boldsymbol{a})$ is then calculated from the Ramsey energy function $h^N_{m,n}(\boldsymbol{a})$ given in Sec. 3 of the manuscript, and its value entered into the appropriate histogram bin. For each Ramsey number experiment, energy histograms are presented over a range of N values. As in Sec. 4 of the manuscript, for each N, two histograms are given. The main histogram shows the energy function in terms of spins variable $\boldsymbol{s}$, where the energy function includes the Ramsey energy and the ferromagnetic interactions enforcing equality constraints between spins representing the same problem variable. The value of the ferromagnetic coupling strength λ used in the quantum annealing runs appears in the upper left corner of this histogram. The inset histogram corresponds to the $\boldsymbol{a}$-configurations, and displays the binned Ramsey energies $E(\boldsymbol{a}) = h^N_{m,n}(\boldsymbol{a})$. It is obtained from the spin configurations (of the main histogram) by filtering out those spin configurations not satisfying the equality constraints as these are infeasible (in the optimization sense) spin configurations. Each inset histogram contains the following information: (i) the set of observed Ramsey energies E, (ii) the probability (relative frequency) for the energy E, and (iii) the number of optimal $\boldsymbol{a}$-configurations that yielded the minimum energy $E = h_{min}$.

Having made these preliminary remarks we examine the remaining Ramsey number results.

A. R(3,3) = 6

As in the manuscript, two histograms are given for each N: the main histogram corresponds to spin energies that include contributions from the Ramsey energy function and the energy penalty functions that enforce the embedding of the primal graph vertices into the chip. As described above, the energy in the inset histograms is the Ramsey energy $h^N_{m,n}(\boldsymbol{a})$. The energy histograms for $R(3,3)$ appear in Fig. 2.

Examining the inset histogram for $N=4$ we see that: (i) $h_{min}=0$; and (ii) 18 distinct $\boldsymbol{a}$-configurations have zero-energy, corresponding to 18 distinct graphs with no 3-cliques or 3-independent sets. From the main histogram we see that the probability to find an optimal $\boldsymbol{a}$-configuration is approximately 0.93. Note that $h_{min}=0$ is exactly the $N=4$ final ground-state energy $E_{gs}(t_f)=0$ found in Ref. 1, indicating that quantum annealing (QA) finds the final ground-state with high probability. The number of optimal graphs found agrees with that found numerically in Ref. 1.

A similar examination of the main histogram for $N=5$ gives: (i) $h_{min}=0$; and (ii) there are 12 optimal graphs/$\boldsymbol{a}$-configurations. From the main histogram we see that the probability to find an optimal $\boldsymbol{a}$-configuration is

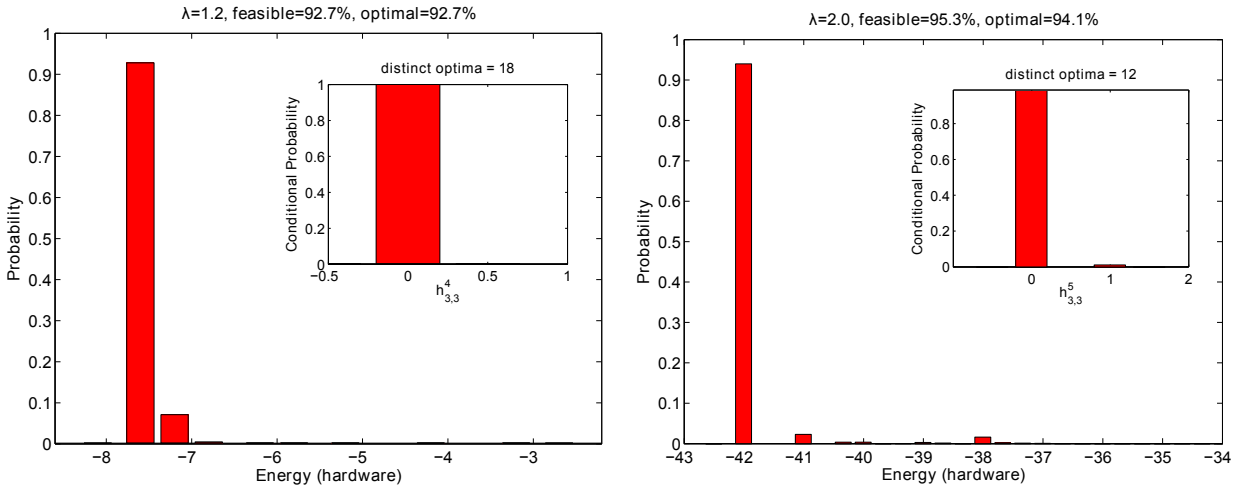

(a) $N = 4$ (b) $N = 5$

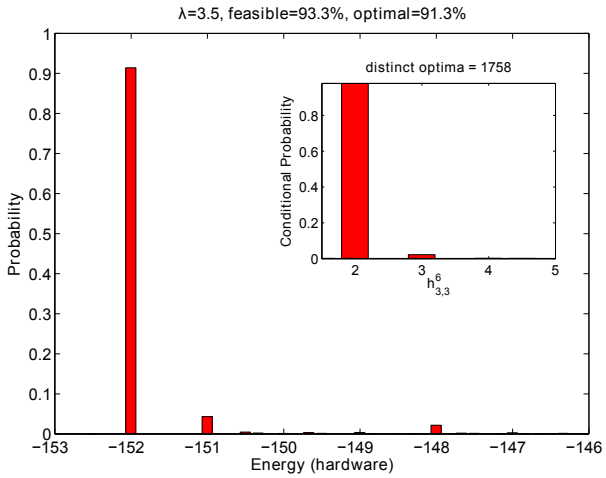

(c) $N = 6$

FIG. 2: **Energy histograms for** $R(3,3)$ **with** $N = 4, 5, 6$**.**

approximately 0.94. Again, $h_{min} = 0$ equals the $N = 5$ ground-state energy $E_{gs}(t_f) = 0$ found in Ref. 1, and so QA finds the final ground-state with high probability. The number of optimal graphs found experimentally agrees with that found numerically in Ref. 1.

For $N = 6$, we see that: (i) $h_{min} = 2$; and (ii) 1758 optimal graphs were observed. From the main histogram we see that the probability to find an optimal $\boldsymbol{a}$-configuration is approximately 0.91. As shown in Ref. 1, $E_{gs}(t_f) = 2$ for $N = 6$, and so $h_{min} = E_{gs}(t_f)$, and QA again finds the final ground-state with high probability. Since $N = 6$ is the first N value for which $h_{min} = E_{gs}(t_f) > 0$, the protocol for the Ramsey quantum algorithm correctly[4] identifies $R(3,3) = 6$. Finally, Ref. 1 showed that the number of optimal graphs for $N = 6$ is 1760 so that QA found all but two of the 1760 optimal graphs.

Table I summarizes all of the above results.

B. $\mathbf{R(m, 2) = m}$

Here we present our experimental results for $R(m,2)$ with $4 \leq m \leq 7$. The results for $m = 8$ appear in the manuscript. Since the $R(m,2)$ discussion closely parallels that of $R(3,3)$, we give a more abbreviated presentation. In the manuscript we showed that for $N < m$, the cost function $h^N_{m,2}(\boldsymbol{a})$ is linear in $\boldsymbol{a}$ and consequently the spins are uncoupled when this cost function is translated to spin variables $\boldsymbol{s}_a$. There is thus no need to introduce ancillary $\boldsymbol{s}_b$-spins,

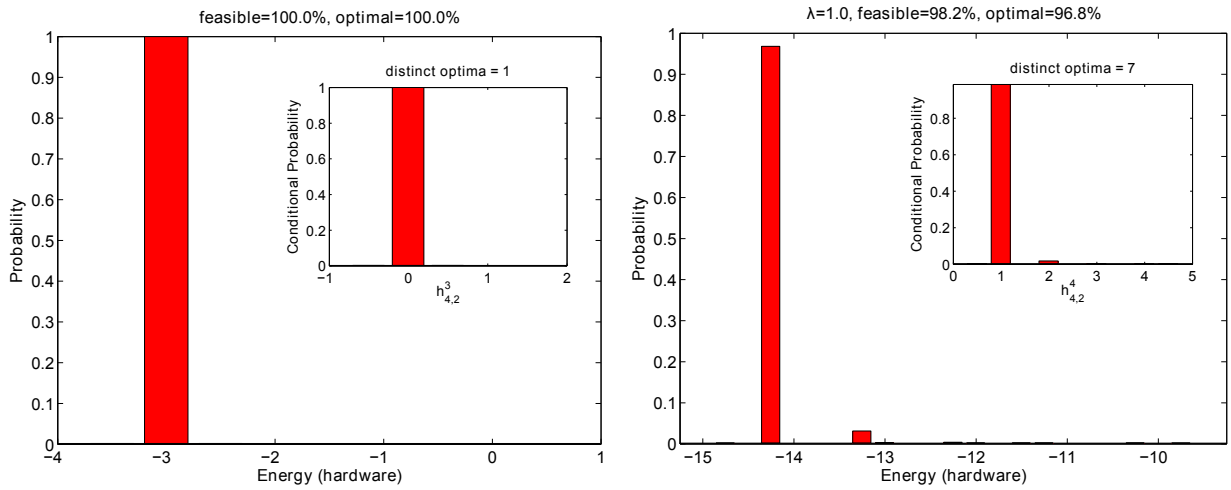

(a) $N = 3$ (b) $N = 4$

FIG. 3: **Energy histograms for $R(4,2)$ with $N = 3$ and 4.**

nor do we need to include ferromagnetic equality penalties in the Ising model. For this reason all spin configurations are feasible for $N < m$, and no λ values are recorded in the main histograms. All results below are included in Table I.

R(4, 2) : Fig. 3 contains the energy histograms for $R(4,2)$. Examining the inset histogram for $N = 3$ (4), we see that: (i) $h_{min} = 0$ (1); (ii) the number of optimal graphs is 1 (7); and (iii) from the main histogram, the probability to find an optimal $\boldsymbol{a}$-configuration is approximately 1.0 (0.97). The minimum energies $h_{min} = 0$ and 1 for $N = 3$ and 4 agree exactly with the corresponding final ground-state energies $E_{gs}(t_f)$ found in Ref. 1, indicating that QA finds the final ground-state with high probability. As h_{min} jumps from $0 \to 1$ as N goes from $3 \to 4$, the Ramsey protocol correctly[4] identifies $R(4,2) = 4$. Finally, Ref. 1 showed that the number of optimal graphs for $N = 3$ and 4 are, respectively, 1 and 7, which agrees with the number of optimals found by QA. For $N = 3$, the unique optimal graph is the fully connected 3-vertex graph which has no 4-cliques or 2-independent sets, while for $N = 4$, the optimal graphs are the $\binom{4}{2} = 6$ graphs with a single 2-independent set and no 4-clique, and the unique fully connected 4-vertex graph which has one 4-clique and no 2-independent set.

R(5, 2) : Fig. 4 contains the energy histograms for $R(5,2)$. Examining the inset histogram for $N = 4$ (5), we see that: (i) $h_{min} = 0$ (1); (ii) the number of optimal graphs is 1 (11); and (iii) from the main histogram, the probability to find an optimal $\boldsymbol{a}$-configuration is approximately 1.0 (0.76). The minimum energies $h_{min} = 0$ and 1 for $N = 4$ and 5 agree exactly with the corresponding final ground-state energies $E_{gs}(t_f)$ found in Ref. 1, indicating that QA finds the final ground-state with high probability. As h_{min} jumps from $0 \to 1$ as N goes from $4 \to 5$, the Ramsey protocol correctly[4] identifies $R(5,2) = 5$. Finally, Ref. 1 showed that the number of optimal graphs for $N = 4$ and 5 are, respectively, 1 and 11, which agrees with the number of optimals found by QA. For $N = 4$, the unique optimal graph is the fully connected 4-vertex graph which has no 5-cliques or 2-independent sets, while for $N = 5$, the optimal graphs are the $\binom{5}{2} = 10$ graphs with a single 2-independent set and no 5-clique, and the unique fully connected 5-vertex graph which has one 5-clique and no 2-independent set.

R(6, 2) : Fig. 5 contains the energy histograms for $R(6,2)$. Examining the inset histogram for $N = 5$ (6), we see that: (i) $h_{min} = 0$ (1); (ii) the number of optimal graphs is 1 (16); and (iii) from the main histogram, the probability to find an optimal $\boldsymbol{a}$-configuration is approximately 1.0 (0.82). The minimum energies $h_{min} = 0$ and 1 for $N = 5$ and 6 agree exactly with the corresponding final ground-state energies $E_{gs}(t_f)$ found in Ref. 1, indicating that QA finds the final ground-state with high probability. As h_{min} jumps from $0 \to 1$ as N goes from $5 \to 6$, the Ramsey protocol correctly[4] identifies $R(6,2) = 6$. Finally, Ref. 1 showed that the number of optimal graphs for $N = 5$ and 6 are, respectively, 1 and 16, which agrees with the number of optimals found by QA. For $N = 5$, the unique optimal graph is the fully connected 5-vertex graph which has no 6-cliques or 2-independent sets, while for $N = 6$, the optimal graphs are the $\binom{6}{2} = 15$ graphs with a single 2-independent set and no 6-clique, and the unique fully connected 6-vertex graph which has one 6-clique and no 2-independent set.

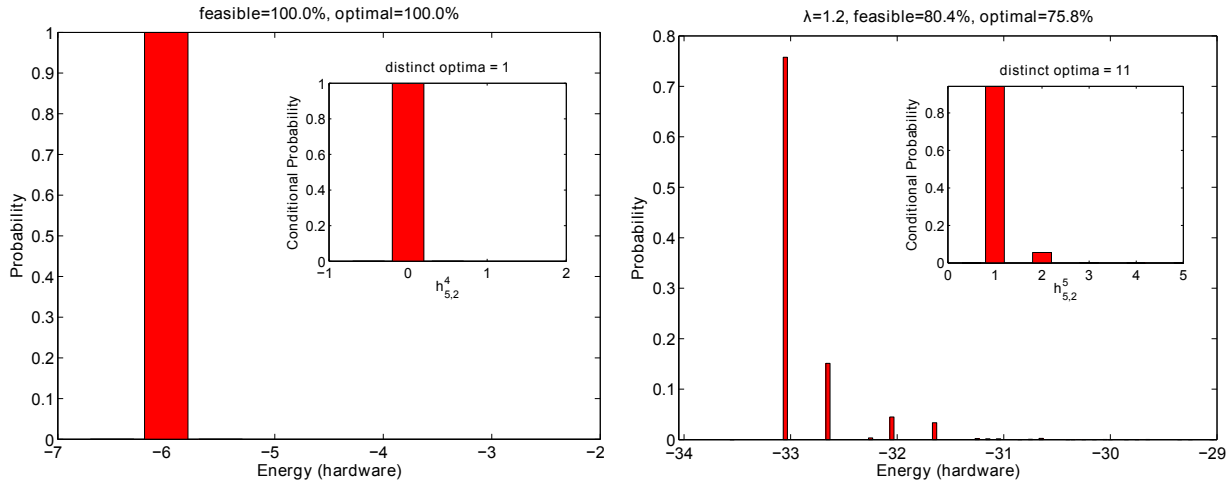

(a) $N = 4$ (b) $N = 5$

FIG. 4: **Energy histograms for $R(5, 2)$ with $N = 4$ and 5.**

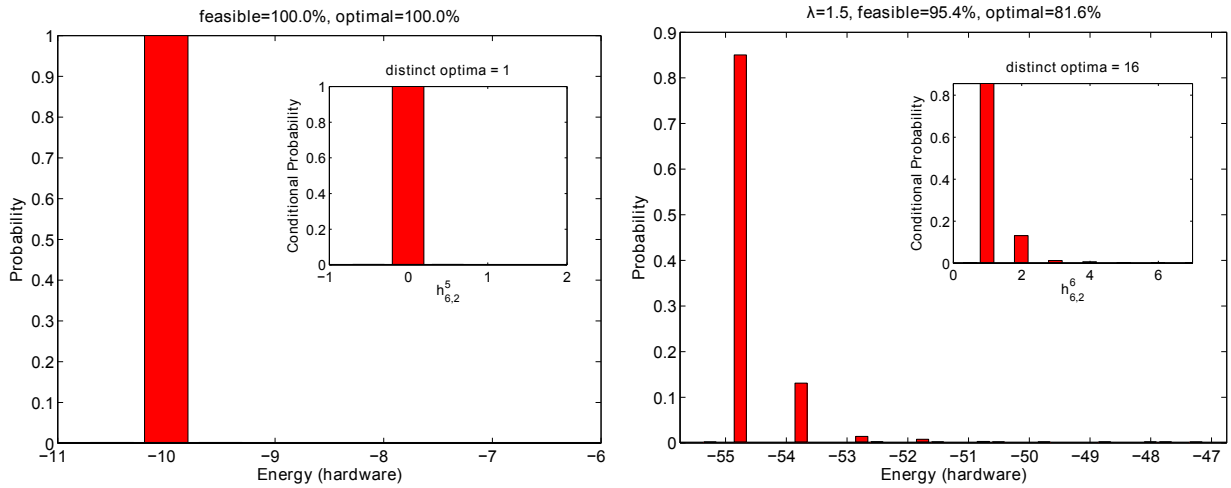

(a) $N = 5$ (b) $N = 6$

FIG. 5: **Energy histograms for $R(6, 2)$ with $N = 5$ and 6.**

R(7, 2) : Finally, Fig. 6 contains the energy histograms for $R(7, 2)$. Examining the inset histogram for $N = 6$ (7), we see that: (i) $h_{min} = 0$ (1); (ii) the number of optimal graphs is 1 (22); and (iii) from the main histogram, the probability to find an optimal $\boldsymbol{a}$-configuration is approximately 1.0 (0.66). The minimum energies $h_{min} = 0$ and 1 for $N = 6$ and 7 agree with the corresponding final ground-state energies $E_{gs}(t_f)$ found in Ref. 1, indicating that QA finds the final ground-state with high probability. As h_{min} jumps from $0 \to 1$ as N goes from $6 \to 7$, the Ramsey protocol correctly[4] identifies $R(7, 2) = 7$. Finally, Ref. 1 showed that the number of optimal graphs for $N = 6$ and 7 are, respectively, 1 and 22, which agrees with the number of optimals found by QA. For $N = 6$, the unique optimal graph is the fully connected 6-vertex graph which has no 7-cliques or 2-independent sets, while for $N = 7$, the optimal graphs are the $\binom{7}{2} = 21$ graphs with a single 2-independent set and no 7-clique, and the unique fully connected 7-vertex graph which has one 7-clique and no 2-independent set.

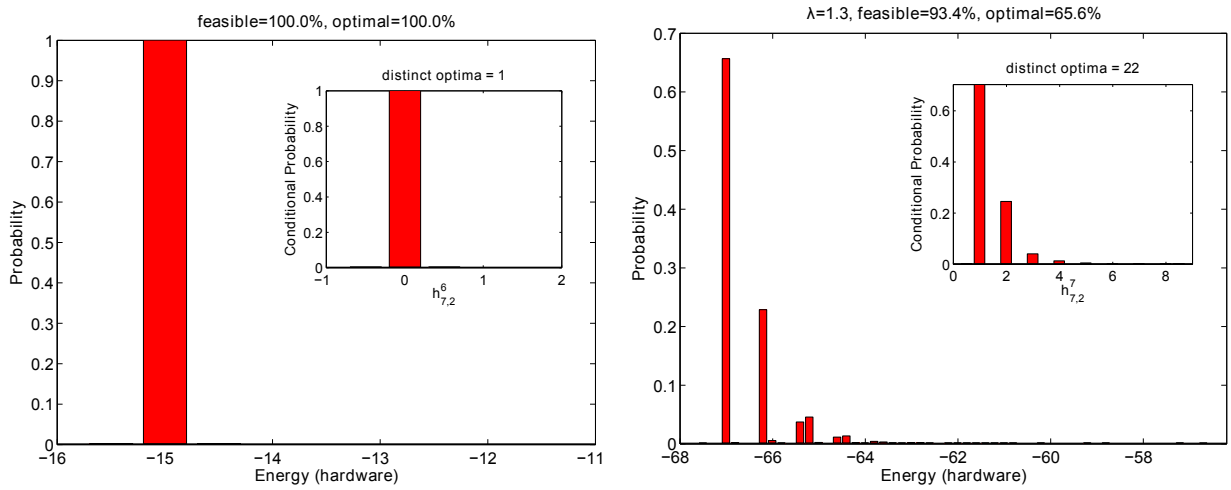

(a) $N = 6$ (b) $N = 7$

FIG. 6: **Energy histograms for $R(7,2)$ with $N = 6$ and 7.**

III. EMBEDDING PRIMAL GRAPH INTO CHIP HARDWARE

Fig. 7 reproduces Fig. 2a of the manuscript which is included here for convenience. Recall that the primal graph of an optimization cost function consists of: (i) vertices that represent bit variables whose values are to be optimized; and (ii) edges that connect pairs of interacting bits. The primal graph of $h^N_{m,n}(\boldsymbol{s})$ is the same as the primal graph of $h^N_{m,n}(\boldsymbol{a})$ as the former is obtained from the latter by the substitution $\boldsymbol{s} = 2\boldsymbol{a} - 1$.

A. R(3,3)

As explained in Section 3 of the manuscript, the cost function $h^6_{3,3}(\boldsymbol{a})$ has 14 variables since we fixed $a_1 = 0$. Fig. 8 shows the embedding of the primal graph for the problem $h^6_{3,3}(0, a_2, a_3, \cdots, a_{15})$. Note that the qubit labeled i in this Figure corresponds to the binary variable a_{i+1}. Like-colored qubits are connected with ferromagnetic couplings of strength λ along the like-colored edges. Black edges are used to represent the coupling strengths between primal variables.The embedding is situated within the chip so that the top-left qubit labeled as 8 in Fig. 8 corresponds to qubit 41 of Fig. 7. Note that many other embeddings into the chip are possible, and we make no claims that this embedding uses the smallest numbers of qubits to represent the required connectivity.

B. R(8,2)

The Ramsey cost function $h^8_{8,2}(\boldsymbol{a})$ is significantly more complex than $R^6_{3,3}$ as it involves a product term that couples 28 spin variables. As discussed in the manuscript this requires the introduction of 26 ancillary $\boldsymbol{b}$-variables to reduce this product to a sum of pairwise interactions. The resulting primal graph for $h^8_{8,2}(\boldsymbol{a}, \boldsymbol{b})$ is shown in Fig. 9 which is a reproduction of Figure 3 in the manuscript. For this case there are a total of 54 primal $\boldsymbol{a}$ and $\boldsymbol{b}$ variables. The embedding of the primal graph in Fig. 9 into the chip is shown in Fig. 10 which is a reproduction of Fig.2b in the manuscript. Note that an additional 30 qubits are needed to complete the embedding, bringing the total number of qubits used in the computation to 84. Like-colored qubits represent a single primal variable, though note that certain colors had to be reused. As before black edges carry the primal variable couplings. The topmost qubit labeled 5 in Fig. 10 corresponds to qubit 17 of Fig. 7.

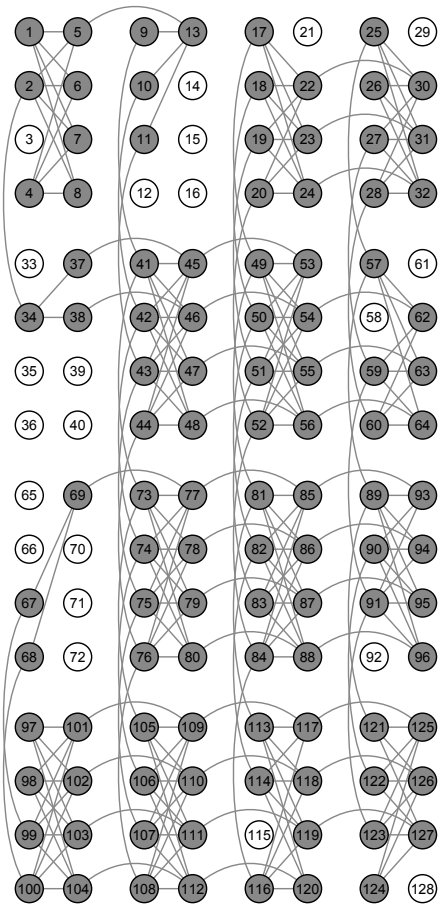

FIG. 7: **Layout of qubits and couplers.** The chip architecture is a 4×4 array of unit cells, with each unit cell containing 8 qubits. Within a unit cell, each of the 4 qubits in the left-hand partition (LHP) connects to all 4 qubits in the right-hand partition (RHP), and vice versa. A qubit in the LHP (RHP) of a unit cell also connects to the corresponding qubit in the LHP (RHP) in the units cells above and below (to the left and right of) it. Most qubits couple to 6 neighbors. Qubits are labeled from 1 to 128, and edges between qubits indicate couplers which may take programmable values. Grey qubits indicate usable qubits, while white qubits indicate qubits which, due to fabrication defects, could not be calibrated to operating tolerances and were not used. All experiments were done on a chip with 106 usable qubits.

C. $\mathbf{R(m, 2)}$ for $\mathbf{4 \leq m \leq 7}$

The procedure for finding the chip embeddings for the Ramsey cost functions $h^m_{m,2}$ with $m = 4, \cdots, 7$ is similar to that presented for $h^8_{8,2}$. The resulting embeddings are much simpler and are not reproduced here.

[1] F. Gaitan & L. Clark. Ramsey numbers and adiabatic quantum computing. *Phys. Rev. Lett.* **108**, 010501 (2012).

[2] E. Farhi, J. Goldstone, S. Gutmann, & M. Sipser. Quantum computation by adiabatic evolution. See http://arxiv.org/abs/quant-ph/0001106, 2000.

[3] J. Spencer, *Ten Lectures on the Probabilistic Method*, 2nd ed. (SIAM, Philadelphia, PA, 1994).

[4] B. Bolloás. *Modern Graph Theory*. Springer, New York, 1998.

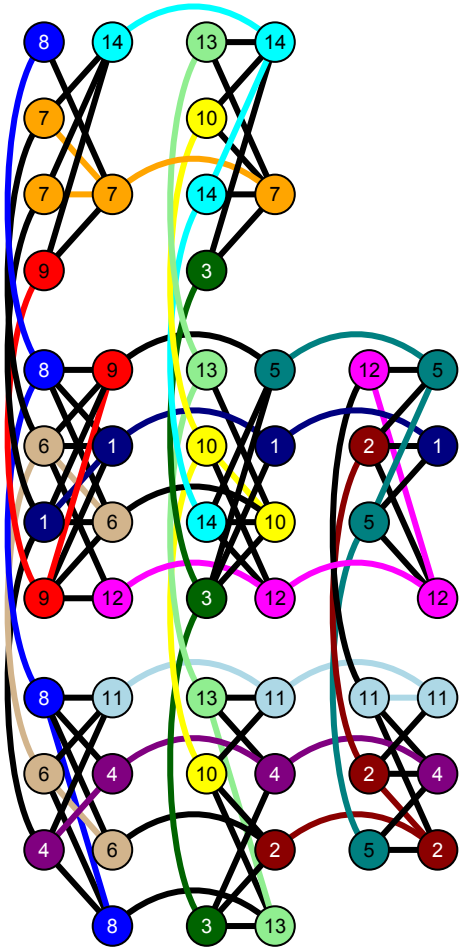

FIG. 8: **Embedding of the primal graph of $h^6_{3,3}(0, a_2, a_3, \cdots, a_{15})$ into hardware.** Variable a_{i+1} is labeled as qubit i.

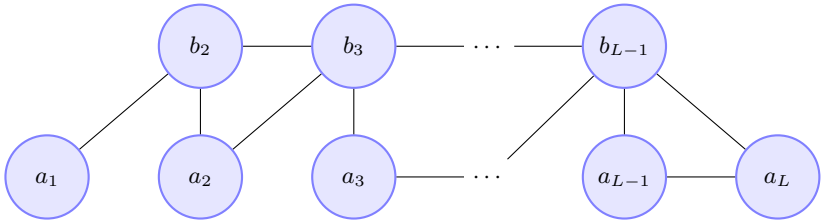

FIG. 9: **Primal graph for $h^m_{m,2}(\boldsymbol{a}, \boldsymbol{b})$.** $L = \binom{m}{2}$ is the total number of $\boldsymbol{a}$ variables.

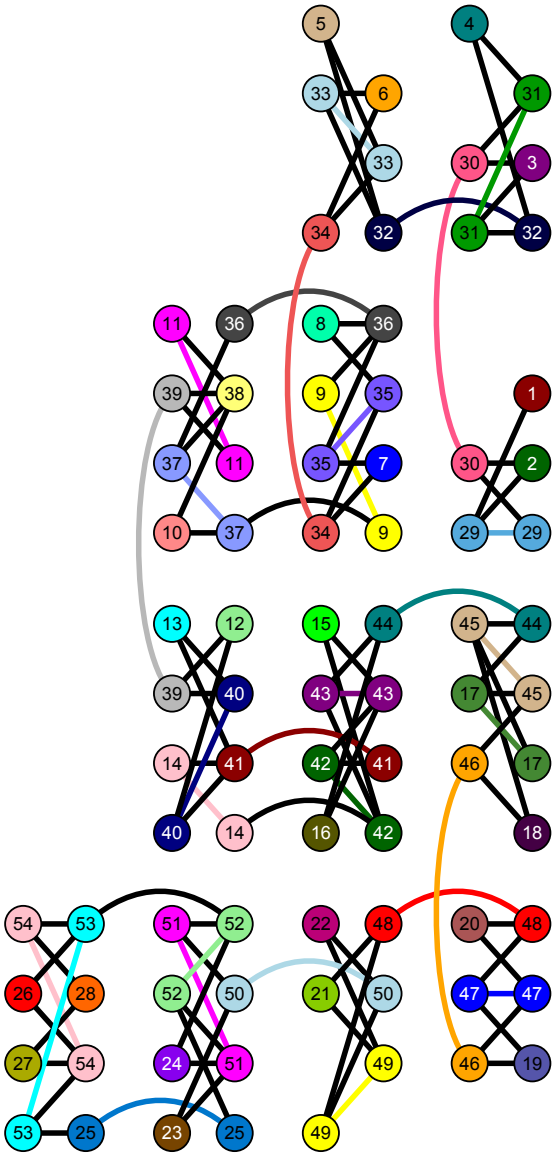

FIG. 10: **Embedding of the primal graph of Fig. 9 into hardware.** Qubits are numbered so that qubits labeled i with $1 \leq i \leq 28$ correspond to primal variables a_i, and qubits labeled $29, \cdots, 54$ correspond to the ancillary variables $b_2, \cdots, b_{27}$.